

Article

Enhancing Corrosion Performance of Cold-Sprayed Titanium/Baghdadite (Ti/BAG) Bio-Composite Coatings via Laser Treatment

Avneesh Kumar, Dhruva Kumar Goyal, Ravi Kant and Harpreet Singh * 

Department of Mechanical Engineering, Indian Institute of Technology Ropar, Rupnagar 140001, India; 2017mez0034@iitrpr.ac.in (A.K.); 2018mez0007@iitrpr.ac.in (D.K.G.); ravi.kant@iitrpr.ac.in (R.K.)

* Correspondence: harpreetsingh@iitrpr.ac.in

Abstract: This study aims to enhance the corrosion performance of cold-sprayed titanium/baghdadite (Ti/BAG) bio-composite coatings. Laser post processing was performed to reduce porosity and improve mechanical properties. The process parameters for laser treatment of cold-sprayed coatings were verified experimentally using scanning electron microscopy (SEM) and a thermal imaging camera. The laser-treated coatings are analyzed with SEM, energy-dispersive spectroscopy (EDS), ImageJ software, and X-ray diffraction (XRD). Furthermore, electrochemical analysis of the laser-treated and as-sprayed coatings was conducted in Ringer's solution. The results of this study revealed that laser treatment helps significantly in enhancing resistance to corrosion for Ti/BAG composite coatings in a Ringer's solution. The reduction in porosity and surface roughness is ascribed as the reason for their superior performance relative to as-sprayed coatings.

Keywords: titanium; baghdadite; cold spray; corrosion; laser treatment; coatings



Citation: Kumar, A.; Goyal, D.K.; Kant, R.; Singh, H. Enhancing Corrosion Performance of Cold-Sprayed Titanium/Baghdadite (Ti/BAG) Bio-Composite Coatings via Laser Treatment. *Coatings* **2022**, *12*, 1010. <https://doi.org/10.3390/coatings12071010>

Academic Editor: Sara Ferraris

Received: 15 June 2022

Accepted: 9 July 2022

Published: 18 July 2022

Publisher's Note: MDPI stays neutral with regard to jurisdictional claims in published maps and institutional affiliations.



Copyright: © 2022 by the authors. Licensee MDPI, Basel, Switzerland. This article is an open access article distributed under the terms and conditions of the Creative Commons Attribution (CC BY) license (<https://creativecommons.org/licenses/by/4.0/>).

1. Introduction

Cold spray is a surface-modification technique widely accepted in industries to enhance the mechanical performance of components. Several surfaces have been coated/repared using cold-spray technology for various applications such as aerospace [1], biomedical [2], power plants [3], and power electronics [4]. For example, biomedical devices are prone to wear and corrosion. Cold spray is widely accepted for developing corrosion and wear-resistant surfaces; therefore, cold-sprayed coatings can be used to overcome these issues. A cold-spray system consists of a De Laval (convergent/divergent) nozzle, which helps to produce a high-velocity jet of processing gas (nitrogen, helium, or compressed air). This high-pressure jet accelerates the feedstock particles in the nozzle to attain supersonic velocity [5]. On impact, metallic particles deform plastically and make mechanical and metallurgical bonds with the substrate/ and adjacent splat [6]. The bonding mechanism of the cold-spray coating is still not clear. Various theories have been given to explain the bonding phenomena, including adiabatic shear instability (ASI) [7,8] and hydrodynamic plasticity [9].

On the other hand, nonmetal particles do not make bonds with the substrate in cold spray due to their poor ductility. Several material combinations have been explored to take the benefits of nonmetals in cold-spray coatings, including metal matrix composite [10,11]. Composite powders are deposited on various substrates, including aluminum, copper, and steel, using cold-spray technology [12–14]. Kumar et al. [15] deposited a metal matrix cold-sprayed composite coating on austenitic stainless-steel (316L SS) substrate for biomedical applications and discussed their microstructure and mechanical and electrochemical behavior. The retention or fracture of ceramic particles into the coatings in cold spray leads to high porosity, which sometimes adversely affects the performance of the cold-spray deposits. The corrosion performance of the cold-spray deposits becomes compromised because of high porosity, providing more surface area to expose with the electrolytic solution [16].

Therefore, surface post-treatment of cold-sprayed deposits can be a promising solution to overcome the above problem. Localized heating of the material in laser treatment makes it the most suitable candidate for the post-treatment of cold-sprayed deposits.

A high-power laser source generates a laser beam to irradiate the coated surface in the laser-treatment process. The irradiated surface forms a melt pool, causing the materials to form better metallurgical bonds [17–19]. As the laser source moves past the melt pool, the material starts solidifying from the solid surface to the melted surface and leads to the development of residual stresses. Zhang and Kong (2018) [20] reported that the developed residual stresses caused by the laser-remelting of cold-spray aluminum coatings on S355 structural steel improve the bonding strength. Sova et al. (2013) [21] deposited austenitic 316L SS on the aluminum substrate using cold spray and discussed the microstructure and mechanical properties before and after remelting of the deposits. They reported that the deposited coatings became denser after laser remelting, which improved the corrosion performance of the coatings. Poza et al. (2014) [22] discussed the laser remelting effect on mechanical properties of Inconel 625 cold-sprayed coatings. They investigated that laser treatment helps in increasing the elastic modulus of the cold-sprayed coatings due to the reduction in porosity. In another work, Marrocco et al. (2011) [23] cold-sprayed titanium (Ti) on carbon steel and then laser-treated the deposited surface to investigate the corrosion behavior change. The results from their study reveal that laser-remelting helped in increasing the resistance to corrosion for the deposited coating by reducing its porosity. The aim of the present work is to explore the influence of laser remelting on the microstructure and mechanical and electrochemical behavior of already-deposited cold-sprayed titanium/baghdadite composite coatings.

2. Experimental Details

Austenitic 316L SS was used as the substrate material for the development of coatings. One face of the substrate was mirror-polished using emery papers down to 2000 grit size, then cleaned with acetone solution. Commercially available titanium (Ti) and baghdadite (BAG) were used as the starting powdered materials for cold spraying. As discussed in our previous work, four distinct compositions were prepared and coated [15]. Once the coatings were deposited, laser post-treatment was performed using a continuous-beam fiber-laser source. Laser post-processing was performed in a protective argon environment to limit the oxidation of the cold-sprayed deposits. The laser parameters used for the optimization of deposited coatings' post-treatment are reported in Table 1. The coating compositions and designations before and after laser treatment are reported in Table 2.

Table 1. Details of the laser-process parameters used for the laser-treatment of Ti/15BAG coating.

Designation	Power (W)	Scanning Speed (mm/min)	Beam Diameter (mm)
500-2000-3	500	2000	3
500-2000-5	500	2000	5
500-3000-5	500	3000	5
400-3000-5	400	3000	5

Table 2. Details of the coatings' composition, designation, and porosity before and after laser treatment.

S. No.	Composition (wt%)		As-Sprayed Coatings		Laser-Treated Coatings	
	Ti	BAG	Designation	Porosity (%)	Designation	Porosity (%)
1	90	10	Ti/10BAG	3 ± 0.003	Ti/10BAG-L	1.19 ± 0.04
2	85	15	Ti/15BAG	4 ± 0.138	Ti/15BAG-L	1.11 ± 0.68
3	80	20	Ti/20BAG	11 ± 0.095	Ti/20BAG-L	1.26 ± 1.33
4	75	25	Ti/25BAG	14 ± 0.993	Ti/25BAG-L	3 ± 1.920

A wire electric-discharge machine (EDM, Electronica, Kolkata, India) was used for sectioning the laser-remelted cold-sprayed deposits. ASTM E-1920 [24] is followed for the sample preparation for the analysis of the laser-remelted deposits. The cut samples were hot-mounted using a hot-mounting machine (Metco, Mumbai, India) with Bakelite powder. The mounted samples were mirror-polished with sandpapers down to 2000 grit to eliminate the effects of cutting. SEM (JEOL, JSM-6610LV, Tokyo, Japan) was used to reveal the microstructure of the laser-treated cold-spray deposits. Further, the phase changes due to laser treatment were analyzed using XRD (Analytical X-pert Pro, Almelo, The Netherlands). EDS (JEOL, JSM-6610LV, Tokyo, Japan) was used to map the elements present in the cold-sprayed coatings after laser remelting. The porosity of the laser-treated coatings was determined by analyzing the SEM micrographs from several sites using ImageJ software. Furthermore, the percentage of BAG retention was calculated by observing EDS micrographs at several sites using ImageJ software. The surface roughness of the as-sprayed and laser-treated coatings was measured by employing a roughness tester in terms of the ten-point height of irregularities (R_z) and arithmetic mean deviation (R_a). Roughness measurements were performed with a cut-off length of 2 mm and a measuring speed of 0.5 mm/s. Ten values of roughness parameters were taken for each coating.

Potentiodynamic corrosion testing was performed to understand the effect of laser treatment on cold-sprayed as-deposited coatings. The Ringer's solution (0.43 g/L KCl, 0.21 g/L NaHCO_3 , 9 g/L NaCl, and 0.24 g/L of CaCl_2) was used as the electrolytic solution for corrosion testing. The testing was carried out using a standard 3-electrode cell (Metrohm Autolab, Utrecht, The Netherlands); specimens as working electrode, silver/silver chloride as reference electrode, and platinum as the counter electrode. The tests were conducted in a potential range of 0.5 V to -0.5 V with a scanning rate of 0.001 V/s and 3600 s of the initial delay. The obtained data were analyzed using NOVA 2.1.3 software with the Tafel extrapolation method.

3. Results and Discussion

Figure 1 shows the results of experimental trials for Ti/15BAG cold-sprayed composite coating. The experimental trials of laser processing were performed on cold-sprayed Ti/15BAG composite coating because of its better mechanical properties than the other investigated coatings [11]. Marrocco et al. [23] optimized laser-process parameters for the Ti deposits of cold spray and reported them in their work. Ti is the major element contributing to the reported composite cold-sprayed coating development in this work. Hence, the work reported by Marrocco et al. [23] is considered a reference for the experimental trials. The parameters were chosen so that the surface temperature of the coating would exceed the recrystallization temperature of Ti and the heat dissipation to the substrate remains minimum.

The process parameters used for experimental trials are reported in Table 1. SEM images of the laser-treated coatings are shown in Figure 1a–d. The melting of the coating and substrate was observed at a power of 500 W, scanning speed of 2000 mm/min, and beam diameter of 3 mm. The maximum surface temperature of the coating measured using a thermal imaging camera was observed 951 °C, which caused damage to the surface of the coating and substrate (Figure 1a,a-1). The change in beam diameter from 3 to 5 mm while keeping the laser power constant caused the heat distribution in larger area. The measured temperature on the surface of the coating in this case was 819 °C, and this led to the removal of the coating from the substrate (Figure 1b,b-1). This may be because of the thermal-expansion mismatch of the coating and substrate. The power of the laser source was reduced from 500 to 400 W, and the scanning speed increased from 2000 to 3000 mm/min by keeping all other parameters the same to reduce the effect of temperature at the interface. The SEM images show that the coating adhered well with the substrate, and inter-particle adhesion/cohesion also improved. The temperature of the coating surface in this case (Figure 1d,d-1) was observed to be 611 °C, which is below the recrystallization temperature of Ti. Therefore, the power of the laser source was changed from 400 to

500 W by keeping all other parameters the same in order to achieve the coating's surface temperature above recrystallization temperature (Figure 1c,c-1). The obtained surface temperature in this case was 743 °C; SEM analysis revealed that there was no adverse effect at the interface because of this localized heating. Hence, all other cold-sprayed composite coatings were laser-treated using the same laser parameters. Figure 1e shows the temperature distribution profile with time. It specifies the influence of scanning speed and beam diameter on maximum temperature of coatings. The higher the scanning speed, the lesser the interaction time between the laser beam and coating surface, leading to a minor heating effect and lower temperature. Similarly, a larger beam diameter will distribute heat in relatively more area leading to a lesser heating effect and lower temperature.

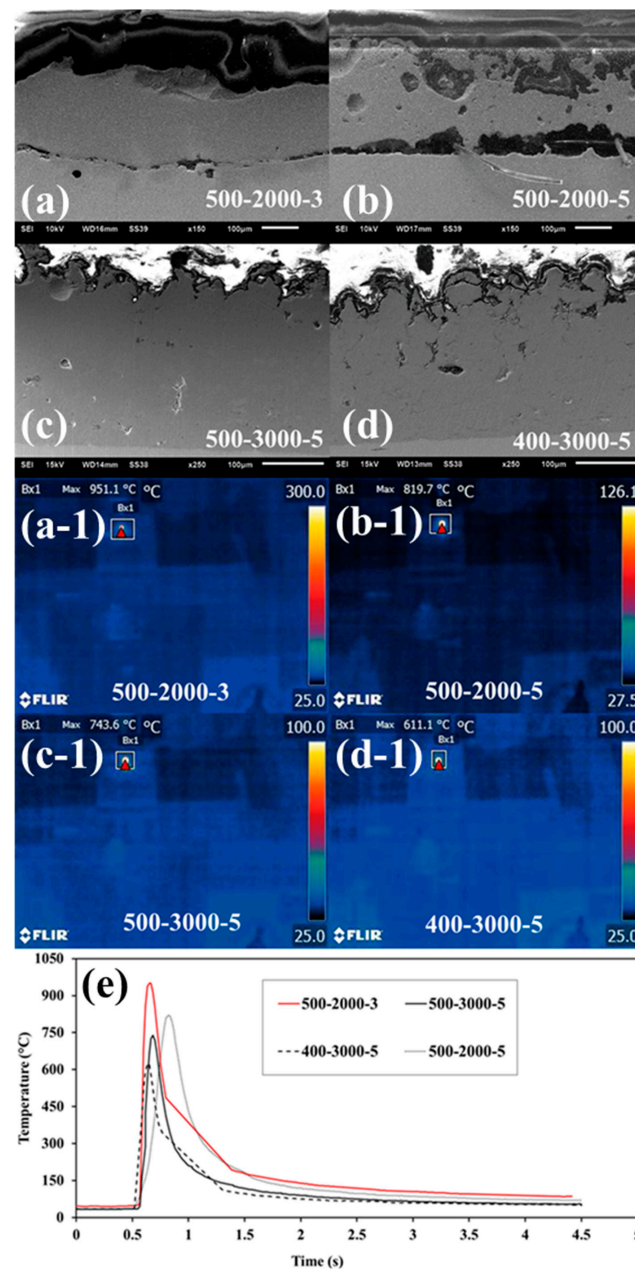


Figure 1. Experimentally measured maximum temperature results of laser-treated cold-sprayed Ti/15BAG composite coating along with SEM images at different laser parameters (a,a-1) 500-2000-3 (b,b-1) 500-2000-5 (c,c-1) 500-3000-5 (d,d-1) 400-3000-5 and (e) temperature distribution profile.

Our previous work discussed the microstructural characterization of as-sprayed coatings [15]. The cross-sectional SEM/EDS micrographs of the laser-treated coatings are

shown in Figure 2. The retention of BAG is visible in the coating. It is observed from the images that the distribution of BAG is non-uniform in the Ti matrix. The percentage retention of the BAG was calculated by analyzing the EDS maps from a different location using ImageJ software. It is observed that the BAG was retained from 65%–80%, depending upon the feedstock composition. The thickness of the as-sprayed coatings ranged from 153–260 μm . The maximum coating thickness was observed for Ti/10BAG cold-sprayed composite coating, and it was found to decrease with the increase in BAG content. Cross-sectional SEM/EDS images of laser-treated coatings revealed that all the coatings' adhesion/cohesion improved except Ti/25BAG. There was a thick crack observed at the Ti/25BAG coating interface. This is because lower coating thickness in this case relative to other cases may have led to the dissipation of higher thermal energy to the substrate under the same laser-processing conditions. This may further be caused by the thermal-expansion mismatch of coating and substrate material. Hence, a crack formed at the interface.

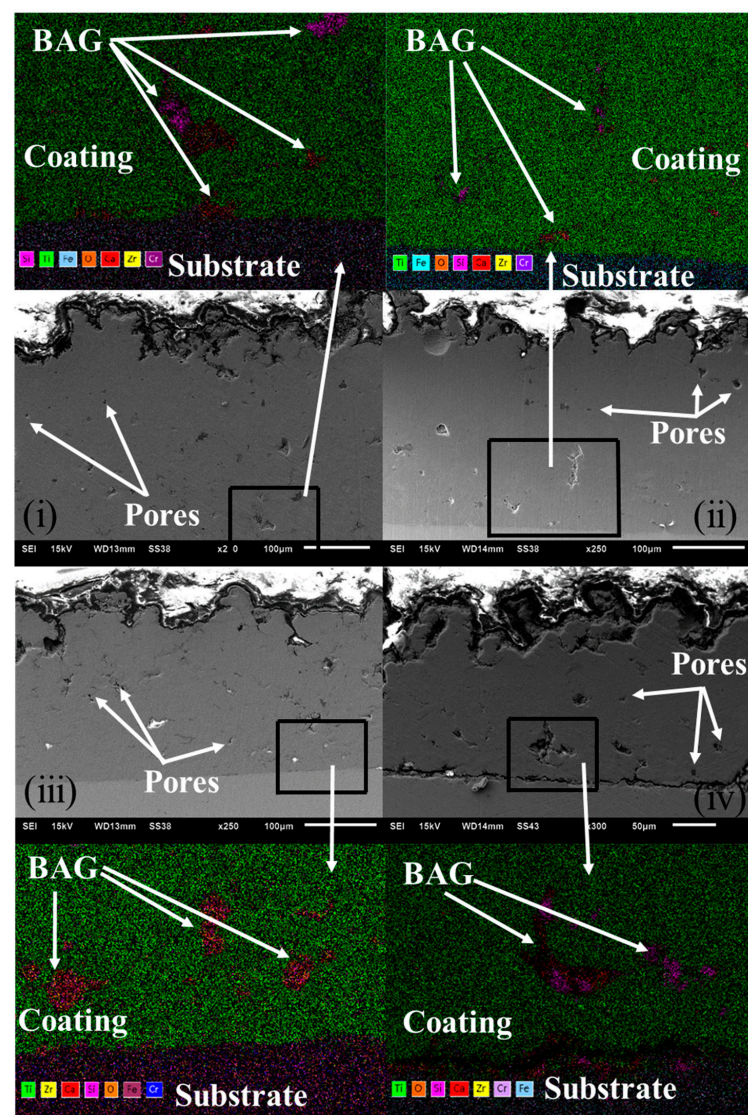


Figure 2. High-magnification SEM/EDS cross-sectional images of the laser-treated cold-sprayed deposits on austenitic 316L SS. (i) Ti/10BAG-L; (ii) Ti/15BAG-L; (iii) Ti/20BAG-L; (iv) Ti/25BAG-L.

The porosity of the coatings was calculated by analyzing the high-magnification SEM cross-sectional micrographs at different locations using ImageJ software. It was observed from the analysis that the BAG content influenced the porosity, as reported in Table 2. The

porosity of the coatings increased with the increment in BAG content. This is attributed to the interaction of the BAG particle with the substrate/and Ti particle. It is well-known that the ceramic (BAG in this case) particle does not make any bond with the adjacent particle/substrate in cold spraying and leaves voids/gaps at the inter-splat boundaries [25]. After laser treatment, the porosity of the coatings reduced significantly, and for all the cases, it went below 2% except for Ti/25BAG-L, as shown in Table 2. This reduction in porosity in laser-treated coatings is caused by the improvement in interparticle adhesion/cohesion caused by the high-temperature remelting of the particles.

Figure 3 shows the top surface SEM micrographs of the as-sprayed and laser-remelted cold-sprayed coatings. The surface pores over the surface of the coatings are visible in the as-deposited coatings. Partial remelting of the deformed particles due to laser irradiation is clearly visible from the surface micrographs, which also helped in reducing the surface pores. Moreover, remelting of the coatings also influenced the surface roughness of the cold-sprayed deposits, as reported in Table 3.

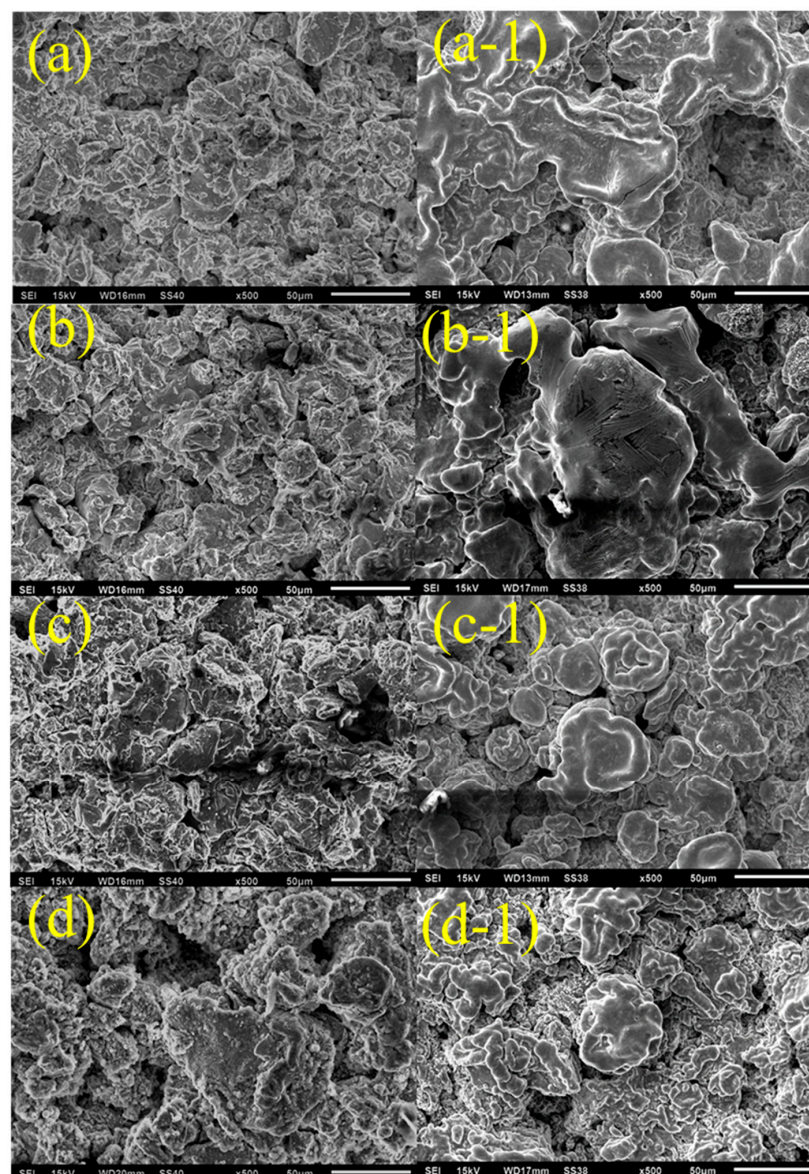
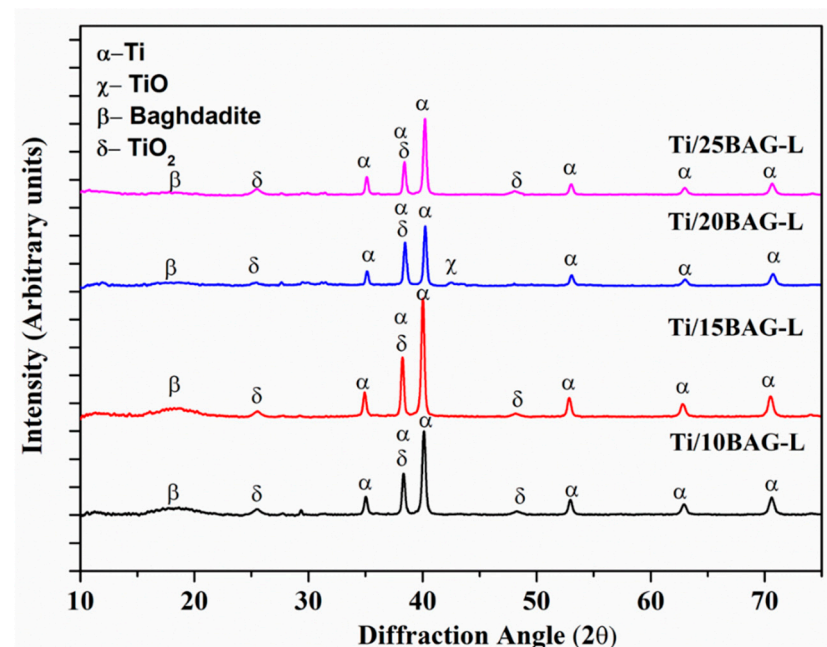


Figure 3. Surface SEM/EDS images of the cold-spray deposits on biomedical steel. (a) Ti/10BAG, (b) Ti/15BAG, (c) Ti/20BAG, (d) Ti/25BAG; and laser-treated coatings (a-1) Ti/10BAG-L, (b-1) Ti/15BAG-L, (c-1) Ti/20BAG-L, (d-1) Ti/25BAG-L.

Table 3. Surface roughness analysis of the cold-sprayed coatings before and after laser treatment.

S. No.	As-Sprayed Coatings		Laser-Treated Coatings	
	Ra (μm)	Rz (μm)	Ra (μm)	Rz (μm)
1	12 \pm 2.17	54.3 \pm 4.67	9 \pm 1.08	29.1 \pm 5.19
2	13 \pm 1.24	72.8 \pm 6.15	10 \pm 1.24	34.6 \pm 4.65
3	17 \pm 1.36	86.7 \pm 4.23	12 \pm 3.28	44.5 \pm 3.45
4	21 \pm 3.21	103.2 \pm 8.11	14 \pm 3.96	56.7 \pm 5.83

Phase analysis of the powder and as-sprayed coatings are reported in our previous work [15]. Laser treatment of cold-sprayed coatings leads to a change in the phase of the coatings, which is reported in Figure 4. It was observed from the analysis of the XRD (Figure 4) results that high temperature in laser treatment led to the formation of TiO_2 , even in the presence of Argon gas. Other than this, Ti and BAG peaks are also observed in all the cases.

**Figure 4.** Phase assessment of the laser-treated cold-spray bio composite deposited on austenitic 316L SS.

Electrochemical corrosion analyses of the as-sprayed and laser-treated coatings were performed in Ringer's solution and reported in Figure 5. Potentiodynamic scans of the substrate and as-sprayed coatings revealed that the as-sprayed coatings are effective in shielding the substrate from corrosion in Ringer's solution. Steel substrate shows a corrosion current density (i_{corr}) of $3.24 \mu\text{A}/\text{cm}^2$, whereas as-sprayed Ti/10BAG composite coating shows a current density $2.29 \mu\text{A}/\text{cm}^2$, which is less than the substrate. Furthermore, the value of corrosion current density decreased with the increase in BAG content (Figure 5a). In addition, the increase in BAG content reduced the corrosion potential. On the other hand, the porosity of the cold-sprayed deposits was found to increase with the rise in BAG content. Still, the BAG content in as-sprayed coatings compensates for the porosity effect on corrosion properties. Post corrosion analysis of as-deposited coatings revealed the formation of the protective oxide layer of TiO_2 , CaO , ZrO_2 , and SiO_2 (Figure 6a).

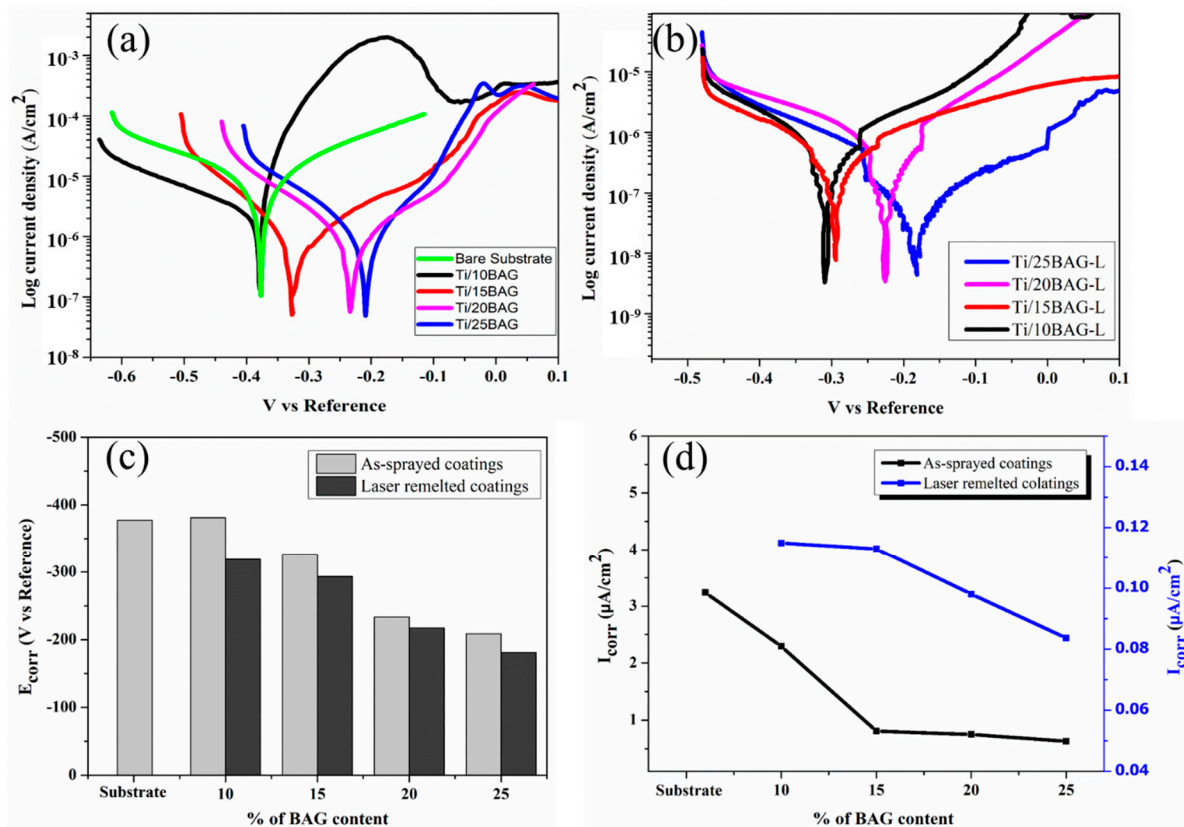


Figure 5. Potentiodynamic scans of (a) as-sprayed (b) laser-treated cold-spray deposits on biomedical steel in Ringer’s solution: (c) E_{corr} and (d) i_{corr} .

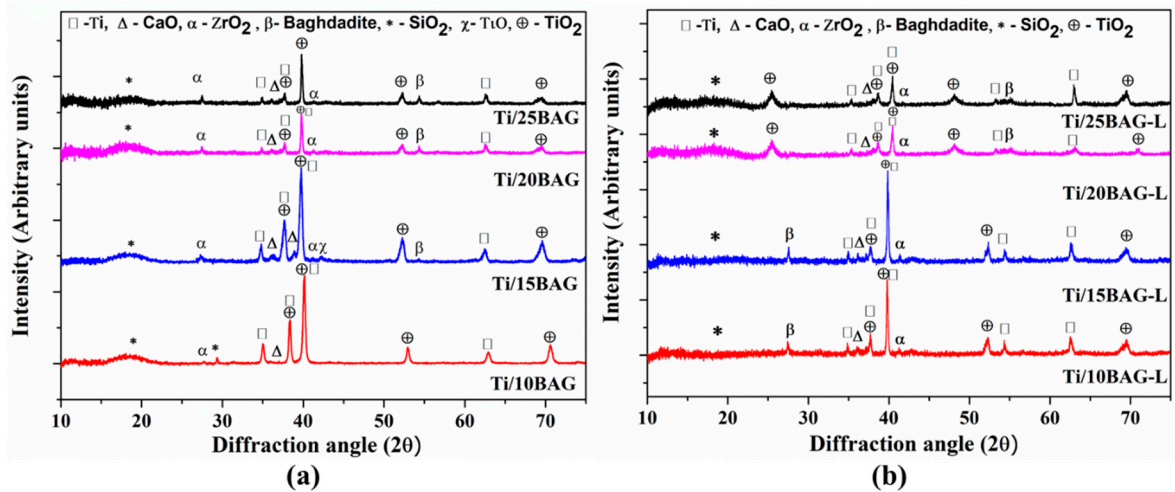


Figure 6. Phase identification of corroded cold-sprayed coatings (a) before laser treatment; (b) after laser treatment.

Potentiodynamic scans of laser-treated coatings reveal that post-laser processing of cold-sprayed deposits helped significantly in reducing the i_{corr} value for each case relative to the as-sprayed coatings, as shown in Figure 5b. The reason for this can be the reduction of porosity and surface roughness due to laser treatment of the cold-sprayed coatings, as discussed earlier. The porosity and surface roughness reduction due to laser treatment decreases the surface area exposed to the Ringer’s solution. Marrocco et al. (2011) [23] reported similar results for laser-treated cold-sprayed Ti coatings. In addition, rougher

surfaces are prone to corrode much faster as they require relatively less energy to lose electrons [26]. Figure 5c,d shows the E_{corr} and i_{corr} value before after laser treatment, which indicates laser-treated coatings are more stable and corrosion-resistant in Ringer's solution.

Post-corrosion XRD analysis of the coatings was performed to understand the reason behind the increase in corrosion resistance of coatings with the rise in BAG content. The results of the investigated corroded samples before and after laser treatments are stated in Figure 6. The analysis reveals that in both the cases (before and after laser treatment), BAG dissolved into Ringer's solution and formed CaO, SiO₂, and ZrO₂. These oxides of Ca, Si, and Zr are well-known to produce a barrier against corrosion [27,28]. The peaks of TiO₂ are also observed in all the cases, indicating the formation of a protective oxide layer over the investigated corroded sample's surfaces. Ti is well-known to provide a barrier to corrosion when exposed to Ringer's solution by forming a stable TiO₂ layer [29].

4. Conclusions

The results demonstrated that BAG influences the porosity of cold-spray Ti/BAG composite coatings. Lack of bonding between ceramic and metallic material in cold spraying is ascribed to the reason for this. Among all the trials, laser power of 500 W, scanning speed of 3000 mm/min, and beam diameter of 5 mm are recommended for optimum remelting of cold-sprayed coatings without deteriorating the substrate. Laser post processing of cold-sprayed Ti/BAG bio composite coatings leads to a substantial reduction in porosity (approximately 60%, 72%, 88%, and 88% for Ti/10BAG, Ti/15BAG, Ti/20BAG, and Ti/25BAG coatings, respectively) and surface roughness (R_a value, approximately 25%, 23%, 29%, and 33% for Ti/10BAG, Ti/15BAG, Ti/20BAG, and Ti/25BAG coatings, respectively) owing to the improvement in bonding between metal–metal and/or metal–ceramic particles. The potentiodynamic polarization tests demonstrated that laser postprocessing helped in improving the corrosion performance of Ti/BAG composite coatings, owing to a reduction in porosity and surface roughness enabling the coatings to be superior barriers to the corrosion species. The i_{corr} value reduced by 94%, 86%, 87%, and 86% for Ti/10BAG, Ti/15BAG, Ti/20BAG, and Ti/25BAG composite coatings, respectively. Moreover, dissolution of BAG into CaO, SiO₂, and ZrO₂ along with the formation of a protective TiO₂ layer over the investigated coating surface into Ringer's solution are ascribed to the reason for the improvement in corrosion resistance of the coatings with the rise in BAG content.

Author Contributions: Conceptualization, A.K., D.K.G. and H.S.; formal analysis, A.K., R.K.; funding acquisition, R.K. and H.S.; investigation, A.K. and R.K.; methodology, A.K., D.K.G., R.K. and H.S.; project administration, H.S.; resources, H.S.; supervision, R.K. and H.S.; validation, A.K., D.K.G., R.K. and H.S.; writing—original draft, A.K.; writing—review and editing, A.K., R.K. and H.S. All authors have read and agreed to the published version of the manuscript.

Funding: This research received no external funding.

Institutional Review Board Statement: Not applicable.

Informed Consent Statement: Not applicable.

Data Availability Statement: Not applicable.

Acknowledgments: The laser system used for this study was established through the Department of Science and Technology, India, under project number DST/TDT/AMT/2017/026. The authors would also like to thank Ram Singh Yadav for helping us with the experiments.

Conflicts of Interest: No potential conflict of interest were reported by the author(s).

References

1. MacDonald, D.; Fernández, R.; Delloro, F.; Jodoin, B. Cold Spraying of Armstrong Process Titanium Powder for Additive Manufacturing. *J. Therm. Spray Technol.* **2017**, *26*, 598–609. [CrossRef]
2. Martín Vilardell, A. Nùria Cinca Luis (dir. tes.), Irene García Cano (dir. tes.), Functionalized Coatings by Cold Spray for Joint Prosthesis. 2017. Available online: <https://dialnet.unirioja.es/servlet/tesis?codigo=230430&orden=0&info=link%0Ahttps://dialnet.unirioja.es/servlet/exttes?codigo=230430> (accessed on 20 May 2022).

3. Bala, N.; Singh, H.; Karthikeyan, J.; Prakash, S. Performance of cold sprayed Ni-20Cr and Ni-50Cr coatings on SA 516 steel in actual industrial environment of a coal fired boiler. *Mater. Corros.* **2013**, *64*, 783–793. [[CrossRef](#)]
4. Archambault, G.; Jodoin, B.; Gaydos, S.; Yandouzi, M. Metallization of carbon fiber reinforced polymer composite by cold spray and lay-up molding processes. *Surf. Coat. Technol.* **2016**, *300*, 78–86. [[CrossRef](#)]
5. Singh, S.; Raman, R.K.S.; Berndt, C.C.; Singh, H. Influence of cold spray parameters on bonding mechanisms: A review. *Metals* **2021**, *11*, 2016. [[CrossRef](#)]
6. Hussain, T.; McCartney, D.G.; Shipway, P.H.; Zhang, D. Bonding Mechanisms in Cold Spraying: The Contributions of Metallurgical and Mechanical Components. *J. Therm. Spray Technol.* **2009**, *18*, 364–379. [[CrossRef](#)]
7. Assadi, H.; Gärtner, F.; Stoltenhoff, T.; Kreye, H. Bonding mechanism in cold gas spraying. *Acta Mater.* **2003**, *51*, 4379–4394. [[CrossRef](#)]
8. Schmidt, T.; Gärtner, F.; Assadi, H.; Kreye, H. Development of a generalized parameter window for cold spray deposition. *Acta Mater.* **2006**, *54*, 729–742. [[CrossRef](#)]
9. Hassani-Gangaraj, M.; Veysset, D.; Champagne, V.K.; Nelson, K.A.; Schuh, C.A. Adiabatic shear instability is not necessary for adhesion in cold spray. *Acta Mater.* **2018**, *158*, 430–439. [[CrossRef](#)]
10. Shockley, J.M.; Descartes, S.; Vo, P.; Irissou, E.; Chromik, R.R. The influence of Al₂O₃ particle morphology on the coating formation and dry sliding wear behavior of cold sprayed Al-Al₂O₃ composites. *Surf. Coat. Technol.* **2015**, *270*, 324–333. [[CrossRef](#)]
11. Kumar, A.; Kant, R.; Singh, H. Tribological Behavior of Cold-Sprayed Titanium/Baghdadite Composite Coatings in Dry and Simulated Body Fluid Environments. *Surf. Coat. Technol.* **2021**, *425*, 127727. [[CrossRef](#)]
12. Kliemann, J.O.; Gutzmann, H.; Gärtner, F.; Hübner, H.; Borchers, C.; Klassen, T. Formation of cold-sprayed ceramic titanium dioxide layers on metal surfaces. *J. Therm. Spray Technol.* **2011**, *20*, 292–298. [[CrossRef](#)]
13. Chen, H.; Pala, Z.; Hussain, T.; McCartney, D.G. Fabrication and microstrain evolution of al-tib2 composite coating by cold spray deposition. *Proc. Inst. Mech. Eng. Part. L J. Mater. Des. Appl.* **2019**, *233*, 1044–1052. [[CrossRef](#)]
14. Zhou, X.; Mohanty, P. Electrochemical behavior of cold sprayed hydroxyapatite/titanium composite in Hanks' solution. *Electrochim. Acta* **2012**, *65*, 134–140. [[CrossRef](#)]
15. Kumar, A.; Singh, H.; Kant, R.; Rasool, N. Development of Cold Sprayed Titanium/Baghdadite Composite Coating for Bio-implant Applications. *J. Therm. Spray Technol.* **2021**, *30*, 2099–2116. [[CrossRef](#)]
16. Jacobs, J.J.; Gilbert, J.L.; Urban, R.M. Corrosion of metal orthopaedic implants. *J. Bone Jt. Surg. Ser. A* **1998**, *80*, 268–282. [[CrossRef](#)]
17. Singh, R.; Martin, M.; Dahotre, N.B. Influence of laser surface modification on corrosion behavior of stainless steel 316L and Ti-6Al-4V in simulated biofluid. *Surf. Eng.* **2005**, *21*, 297–306. [[CrossRef](#)]
18. Olakanmi, E.O. Optimization of the Quality Characteristics of Laser-Assisted Cold-Sprayed (LACS) Aluminum Coatings with Taguchi Design of Experiments (DOE). *Mater. Manuf. Process.* **2016**, *31*, 1490–1499. [[CrossRef](#)]
19. Jing, Z.; Dejun, K. Effect of laser remelting on friction-wear behaviors of cold sprayed Al coatings in 3.5% NaCl solution. *Materials* **2018**, *11*, 283. [[CrossRef](#)]
20. Zhang, J.; Kong, D. Effect of laser remelting on microstructure and immersion corrosion of cold-sprayed aluminum coating on S355 structural steel. *Opt. Laser Technol.* **2018**, *106*, 348–356. [[CrossRef](#)]
21. Sova, A.; Grigoriev, S.; Okunkova, A.; Smurov, I. Cold spray deposition of 316L stainless steel coatings on aluminium surface with following laser post-treatment. *Surf. Coat. Technol.* **2013**, *235*, 283–289. [[CrossRef](#)]
22. Poza, P.; Múñez, C.J.; Garrido-Maneiro, M.A.; Vezzù, S.; Rech, S.; Trentin, A. Mechanical properties of Inconel 625 cold-sprayed coatings after laser remelting. Depth sensing indentation analysis. *Surf. Coat. Technol.* **2014**, *243*, 51–57. [[CrossRef](#)]
23. Marrocco, T.; Hussain, T.; McCartney, D.G.; Shipway, P.H. Corrosion performance of laser posttreated cold sprayed titanium coatings. *J. Therm. Spray Technol.* **2011**, *20*, 909–917. [[CrossRef](#)]
24. ASTM International E1920-03. Standard guide for metallographic preparation of thermal sprayed coatings. *Current* **1920**, *3*, 1–5.
25. Zhang, Z.; Liu, F.; Han, E.H.; Xu, L.; Uzoma, P.C. Effects of Al₂O₃ on the microstructures and corrosion behavior of low-pressure cold gas sprayed Al 2024-Al₂O₃ composite coatings on AA 2024-T3 substrate. *Surf. Coat. Technol.* **2019**, *370*, 53–68. [[CrossRef](#)]
26. Li, W.; Li, D.Y. Influence of surface morphology on corrosion and electronic behavior. *Acta Mater.* **2006**, *54*, 445–452. [[CrossRef](#)]
27. Catauro, M.; Dell'Era, A.; Cipriotti, S.V. Synthesis, structural, spectroscopic and thermoanalytical study of sol-gel derived SiO₂-CaO-P₂O₅ gel and ceramic materials. *Thermochim. Acta* **2016**, *625*, 20–27. [[CrossRef](#)]
28. Catauro, M.; Barrino, F.; Bononi, M.; Colombini, E.; Giovanardi, R.; Veronesi, P.; Tranquillo, E. Coating of titanium substrates with ZrO₂ and ZrO₂-SiO₂ composites by sol-gel synthesis for biomedical applications: Structural characterization, mechanical and corrosive behavior. *Coatings* **2019**, *9*, 200. [[CrossRef](#)]
29. Marino, C.E.B.; de Oliveira, E.M.; Rocha-Filho, R.C.; Biaggio, S.R. On the stability of thin-anodic-oxide films of titanium in acid phosphoric media. *Corros. Sci.* **2001**, *43*, 1465–1476. [[CrossRef](#)]